Competition between Antiferromagnetism and Superconductivity in the Electron-Doped Cuprates Triggered by Oxygen Reduction

P. Richard,[1,*] M. Neupane,[1] Y.-M. Xu,[1] P. Fournier,[2] S. Li,[3] Pengcheng Dai,[3,4] Z. Wang,[1] and H. Ding[1]

[1]*Department of Physics, Boston College, Chestnut Hill, Massachusetts 02467, USA*

[2]*Département de physique, Université de Sherbrooke, Sherbrooke, Québec, Canada, J1K 2R1*

[3]*Department of Physics and Astronomy, The University of Tennessee, Knoxville, Tennessee 37996, USA*

[4]*Neutron Scattering Sciences Division, Oak Ridge National Laboratory, Oak Ridge, Tennessee 37831, USA*

(Received 2 April 2007; published 11 October 2007)

We have performed a systematic angle-resolved photoemission study of as-grown and oxygen-reduced $Pr_{2-x}Ce_xCuO_4$ and $Pr_{1-x}LaCe_xCuO_4$ electron-doped cuprates. In contrast with the common belief, neither the band filling nor the band parameters are significantly affected by the oxygen reduction process. Instead, we show that the main electronic role of the reduction process is to remove an anisotropic leading edge gap around the Fermi surface. While the nodal leading edge gap is induced by long-range antiferomagnetic order, the origin of the antinodal one remains unclear.

DOI: 10.1103/PhysRevLett.99.157002 PACS numbers: 74.72.Jt, 74.25.Jb, 74.62.Dh, 79.60.−i

The CuO_2 plane of cuprates, where high-T_c superconductivity is believed to occur, can be doped either by holes or electrons. Even though most of the work has been focused on hole-doped materials, the understanding of their electron-doped counterparts is essential for obtaining a universal picture of high-T_c superconductivity. To achieve this goal and make sure that the intrinsic properties of the electron-doped CuO_2 planes are studied, it is necessary to first solve the main mystery that holds since the discovery of the T'-structure electron-doped cuprates $RE_{2-x}Ce_xCuO_4$ and $RE_{1-x}LaCe_xCuO_4$ (RE = Pr, Nd, Sm, Eu): why is superconductivity in these compounds achieved *only* when a tiny amount of oxygen (~1%) is removed from the as-grown (AG) samples following a post-annealing process (reduction) [1–5]? In fact, the reduction process has a drastic impact on the transport properties: for adequate doping regime, it modifies the low temperature behavior of the in-plane resistivity from insulating to metallic and superconducting (SC) and has a significant impact on the Hall coefficient, which can even show a sign change [6].

Even though the microscopic origin of the reduction process is still under intense debate, the proximity of the antiferromagnetic (AF) and SC phases suggests that the interplay between the AF and SC states is strongly affected by this process. Indeed, the appearance of the SC dome is accompanied by a significant drop of the Néel temperature [7] and long-range AF can eventually disappear in the optimally doped and fully reduced samples [7,8]. Understanding how the reduction process can trigger the competition between the AF and SC states and modify the electronic band structure is thus crucial.

In this Letter, we present the first systematic angle-resolved photoemission spectroscopy (ARPES) study of the impact of the reduction process in the electron-doped cuprates. We show that neither the electronic filling nor the band structure parameters are significantly changed by the reduction process. Instead, the reduction process suppresses long-range AF order and fills up a leading edge gap (LEG) which has two components. While the nodal LEG is of AF origin, the nature of the antinodal LEG remains unclear.

High-quality single crystals of $Pr_{1.85}Ce_{0.15}CuO_4$ and $Pr_{0.88}LaCe_{0.12}CuO_4$ were grown by the flux and floating zone techniques, respectively. Some of the AG $Pr_{1.85}Ce_{0.15}CuO_4$ and $Pr_{0.88}LaCe_{0.12}CuO_4$ samples, which are all non-SC, have been annealed as described in Refs. [9–11] and they are referred in the text as reduced samples. The reduced samples exhibit SC transitions around 24 K. ARPES experiments were conducted at the PGM and U1-NIM beam lines of the Synchrotron Radiation Center (Stoughton, WI) with photon energies of 73.5 and 22 eV. The data were recorded at 40 K using a Scienta SES-2002 analyzer with a 30 meV energy resolution. The samples were cleaved *in situ* in a vacuum better than 10^{-10} Torr. Although this Letter focuses on the data obtained on $Pr_{2-x}Ce_xCuO_4$, similar results have been obtained for the $Pr_{1-x}LaCe_xCuO_4$ samples.

In order to transform AG samples into superconductors, the reduction process must affect the electronic structure and especially the excitations near the Fermi energy (E_F). Figure 1 compares the constant energy intensity plots (CEIPs) of the reduced 1(a) and 1(b) and AG 1(d) and 1(e) samples in momentum space, as obtained by ARPES. Bright spots indicate regions with large photoemission intensity. The CEIPs centered at −100 meV with 20 meV energy integration window 1(b) and 1(e) are quite similar, and one can easily distinguish the $X(\pm\pi, \pm\pi)$-centered holelike pockets. This contrasts with the CEIPs centered at E_F 1(a) and 1(d). Contrary to the reduced sample [Fig. 1(a)], the intensity at E_F is strongly suppressed in the AG sample [Fig. 1(d)]. Nevertheless, underlying Fermi surface (FS) contours can be extracted in both cases and the results are reproduced in Figs. 1(c) and 1(f) for the reduced and AG samples, respectively. Surprisingly, the data extracted for the reduced and the AG samples can be

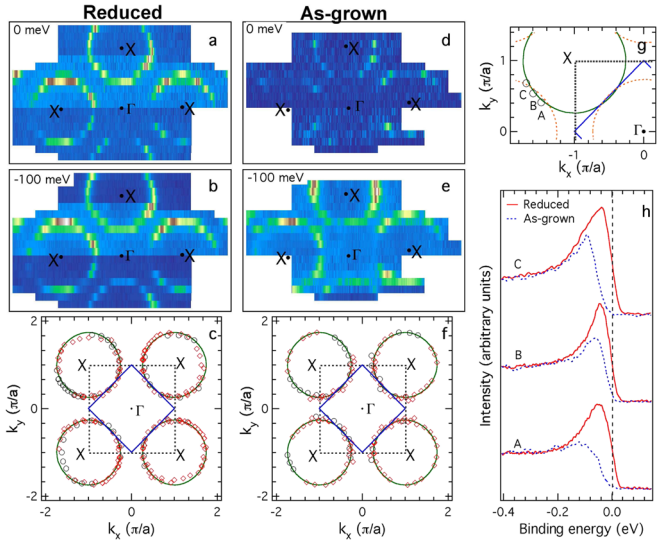

FIG. 1 (color online). (a), (b) and (d), (e) CEIPs (20 meV integration) of the ARPES data obtained at 40 K using 73.5 eV photons with a $\mathbf{A}||\Gamma$-X polarization. (c), (f) Underlying FS contours associated with the reduced and AG samples. The experimental data are represented by circles while the points indicated by diamonds have been obtained by symmetry operations. The data have been fitted by an effective tight-binding model (see the text). (h) Comparison of the EDCs of reduced (solid lines) and AG (dashed lines) at the locations given in panel (g).

fitted, within uncertainties, with the same band parameters $\mu = 0.05$ eV, $t = -1.1$ eV, and $t' = 0.32$ eV, using the simple effective tight-binding (TB) model $E - \mu = t/2[\cos(k_x) + \cos(k_y)] + t' \cos(k_x)\cos(k_y)$.

According to Luttinger theorem, the introduction of extra negative carriers following the reduction would lead to smaller X-centered holelike pockets and thus to at least an increase of μ, which is not observed. Actually, the underlying FS contours coincide with a doping of $x \approx 0.15$ in both cases. This is a strong evidence that the reduction process modifies neither the band filling nor the global shape of the band dispersion sufficiently to induce the dramatic changes observed in the transport properties [6]. Instead, the CEIPs at E_F indicate that the annealing process removes a gap that is present at E_F in the AG samples. This assertion is confirmed by Fig. 1(h), which compares the electron distribution curves (EDCs) of AG and reduced samples at different k locations given in Fig. 1(g). All the AG sample spectra have their leading edge shifted towards higher binding energies as compared with the corresponding reduced sample spectra and thus have much weaker intensities at E_F.

Now one asks the question: how can the reduction process suppress the LEG observed in the AG samples? We first checked that the samples were not charged by increasing the photon flux, which had no influence on the LEG in our experiment. The most likely candidate to explain this mystery is the AF ordering, which exists in AG samples. It is known that AF is suppressed in the reduced samples [7,8]. This effect is clearly observed by ARPES. We plotted in Figs. 2(a) and 2(b) the electronic dispersion as measured along the lines indicated in Fig. 2(c) for the reduced (dashed) and AG (solid) samples, respectively. In addition to the main band branches, indicated with dashed arrows, the spectrum of the AG sample shows features that are not observed in the reduced one. As indicated by solid arrows in Fig. 2(b), these features correspond to the AF-induced folding (AIF) band. Such features, observed in the 1st and 2nd Brillouin zones (BZs), are responsible for the $M(-\pi, 0)$-centered electron FS pockets emphasized in Fig. 2(d), which shows the AG CEIP at -50 meV obtained with 22 eV photons.

In the presence of an AIF band, the hybridization of the main and AIF bands due to the scattering by the AF wave vector opens a gap at locations coinciding with the magnetic BZ boundary [12]. The energy position of the center of the gap between the upper and lower hybridized bands depends on the k location along that boundary, defined by $M(0, \pi)$ and equivalent points. Hence, along the $(0, \pi) \rightarrow (\pi, 0)$ direction, it occurs below E_F between the M points and the hot spots, which are defined as the k locations where the intersection occurs exactly at E_F. On the other hand, between the hot spots, the intersection occurs always above E_F and the upper hybridized band can never cross E_F and therefore cannot be observed by low temperature ARPES, whereas the top of the lower hybridized band is

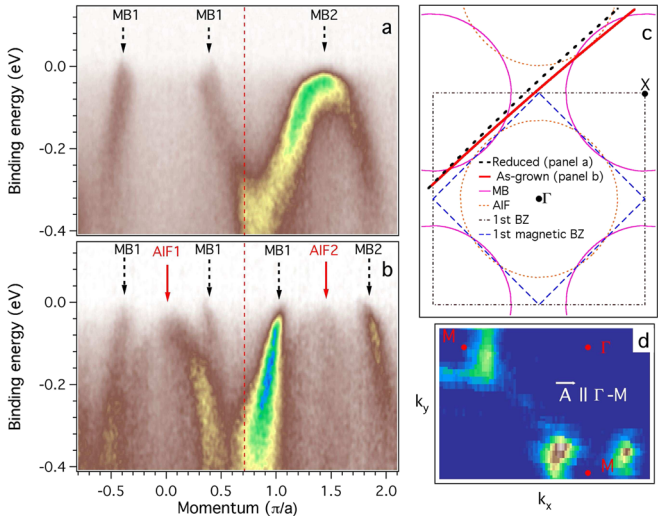

FIG. 2 (color online). Comparison of the reduced (a) and AG (b) spectra obtained along the lines given in (c). MB (dashed arrows) and AIF (solid arrows) indicate the main and AIF band structures, respectively. The vertical dashed line in (a), (b) indicates the AF boundary. The number next to MB or AFI indicates the zone in which the band is detected. (d) CEIP at -50 meV (30 meV integration) of a $Pr_{1.85}Ce_{0.15}CuO_4$ AG sample obtained at 22 eV. The suppression along the vertical Γ-M direction is due to ARPES selection rules.

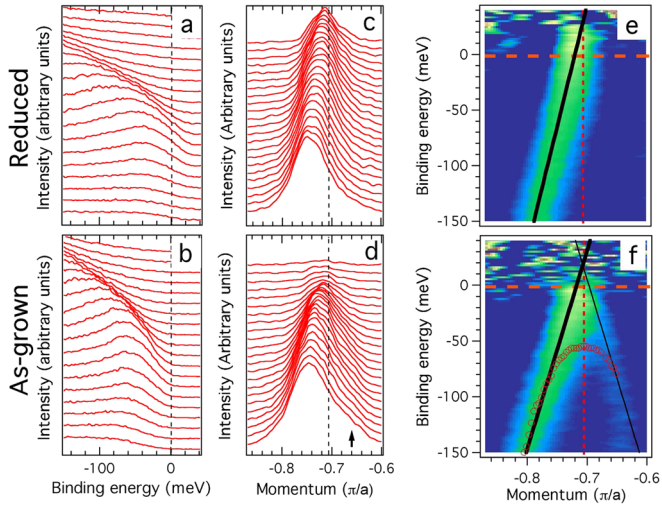

FIG. 3 (color online). Comparison of the nodal dispersion (2nd BZ) between reduced (top panels) and AG samples (bottom panels). (a), (b) EDCs from $-0.62\pi/a$ (bottom) to $-0.87\pi/a$ (top). The vertical line corresponds to E_F. (c), (d) MDCs between -80 meV (bottom) and 0 meV (top). The vertical line indicates the AF boundary and the arrow an asymmetry suggesting the presence of an extra band. (e), (f) SMDI plots. The vertical dashed line indicates the AF boundary. The thick and thin solid lines indicate the unhybridized main and AF bands, respectively, while the dots correspond to the maximum position of the EDCs (hybridized band).

pushed down. When the AF gap is large enough, the small holelike FS pocket around $(\pi/2, \pi/2)$ is gapped out.

In order to check this scenario, we investigated the band dispersion of reduced and AG samples along the nodal (Γ-X) direction. The results are given in Fig. 3. Figures 3(a) and 3(b) show the EDCs of the reduced and AG samples, respectively. Besides the clear LEG observed for the AG sample as compared to the reduced one, the EDC maxima of the AG sample exhibit a bending back characteristic of hybridization: from the top to the bottom of Fig. 3(b), the EDC maxima first move closer to E_F, and then move away, with a decrease of intensity.

A contrast in the shape of the momentum distribution curves (MDCs) of the reduced and AG samples, which are given, respectively, in Figs. 3(c) and 3(d), is also observed. The asymmetric shape of the AG MDCs suggests the presence of a band folded along the AF boundary (vertical dashed line). This effect is clearly seen in the corresponding second momentum-derivative intensity (SMDI) plots displayed in Figs. 3(e) and 3(f) for the reduced and AG samples, respectively. The position of the MDC peaks corresponds to the minimum in the SMDI plots (bright spots). In contrast to the SC sample, the AG sample exhibits an additional band whose dispersion is the reflection of the main band with respect to the AF boundary. Using the position of the MDCs, we extracted the main band dispersion and reported it in Fig. 3(f), along with its reflection across the AF boundary. We also reported in Fig. 3(f) the position of the EDC maxima associated with the AG sample. These maxima, which coincide with the renormalized dispersion band, support the hybridization scenario and indicate that the portion of the FS around $(\pi/2, \pi/2)$ is suppressed in the AG samples.

Figure 4(a), which compares the k dependence of the leading edge shift for the AG and reduced samples, provides additional evidence that an AF hybridization gap is suppressed after the reduction process. While no clear LEG is observable for the reduced sample, an anisotropic LEG is observed for the AG sample. As expected from the hybridization scenario [12], a maximum is observed around the hot spot. In order to illustrate further the AF scenario, we plotted in Figs. 4(b)–4(e) simulations of the nodal dispersion obtained using the fit parameters given above, with various AF gap sizes. We introduced a broadening to mimic realistic results and removed the Fermi function for sake of clarity. For a large gap, the band folding is clearly observable and the lower hybridized band never crosses E_F. As a consequence, a large LEG is recorded. This LEG decreases as the gap becomes smaller, and it disappears when the lower band crosses E_F, as illustrated in 4(d). Our simulations indicate that a LEG of 20 meV along the nodal direction can be produced by a 60 meV AF LEG at the hot spot with a proper linewidth, in agreement with our observation in Fig. 4(a).

While the experimental results for the nodal region can easily be described by an AF hybridization gap, such a model alone fails to explain the LEG observed for the antinodal region, where the main and AIF bands intersect below E_F. In particular, the original band position at M is $\sim$300 meV below E_F; thus a small LEG ($\sim$20 meV) cannot be produced by a simple AF hybridization effect. Nevertheless, AF order may still be responsible for the antinodal LEG. It has been predicted that the whole FS of the $Nd_{1.85}Ce_{0.15}CuO_4$ SC samples is pseudogapped due to paramagnons in the semiclassical regime, but without a LEG in the antinodal region, where paramagnons only make the signal incoherent [13]. Our experimental data indicate no antinodal LEG for the reduced samples, but do show one in the AG samples, for which the AF correlations are much stronger.

We now turn to a critical question: how can a small amount of extra oxygen atoms induce AF order in the AG samples? Literature provides two opposite scenarios involving CuO_2 plane defects and the AF-SC states competition and the suppression of long-range AF in the reduced samples. Recent Raman and crystal-field infrared transmission studies revealed two main defects appearing with the oxygen reduction, which have been tentatively assigned to out-of-plane and in-plane oxygen vacancies, the latter being the only one observed at optimal doping [9,10]. It has been suggested that in-plane oxygen vacancies in the reduced samples can suppress the AF order, affect the band parameters, and induce superconductivity [9,10]. However, the present study indicates that the band parameters are not

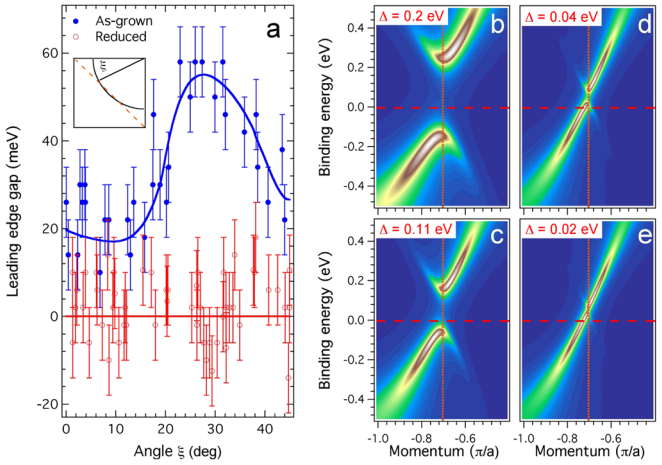

FIG. 4 (color online). (a) k dependece of the LEG given as a function of the angle ξ defined in the inset. Lines are guides for the eye. (b)–(e) Simulations of the nodal band dispersion (2nd BZ) in the presence of an AF gap. The vertical dashed line indicates the AF boundary. We used the TB parameters defined in the text and introduced a band broadening in order to mimic real data.

modified significantly by the reduction process. In this scenario, the antinodal LEG would be more likely an indirect consequence of magnetic fluctuations such as paramagnons [13]. The lack of theoretical study on the subject leaves open the possibility that charge disorder induced by oxygen vacancies can suppress the AF order and promote superconductivity.

An opposite idea is based on recent neutron observation of a $(RE, \mathrm{Ce})_2\mathrm{O}_3$ impurity phase epitaxial to the CuO_2 planes, which appears in the reduced SC samples but disappears in reoxygenated non-SC samples [7,11,14,15]. Based on this phenomenon, it has been proposed that the Cu excess released during the formation of $(RE, \mathrm{Ce})_2\mathrm{O}_3$ fills Cu vacancies and makes the remaining structure more stoichiometric [11]. For hole-doped cuprates, it has been argued that a Cu vacancy, like a nonmagnetic Zn impurity, would suppress local SC phase coherence and at the same time induce a staggered paramagnetic $S = 1/2$ local moment extending over a few unit cells [16]. Such impurity-induced local magnetism has been recently observed by in-plane $^{17}\mathrm{O}$ NMR in the SC state of the optimally hole-doped $\mathrm{YBa_2Cu_3O_7}$ with dilute Zn impurities [17]. If the amount of Cu vacancies in the AG samples is small but sufficient, an AF long-range order can be established by quantum percolation of the AF regions. In addition, the strong scattering of the Cu vacancies in CuO_2 planes of AG samples may produce a localization gap (or Coulomb gap) that could explain the observed antinodal LEG. We note that the residual resistivity ($\sim$500 $\mu\Omega$ cm) at the superconductor-insulator transition found in reoxygenated $\mathrm{Pr_{1.83}Ce_{0.17}CuO_4}$ thin films [6] corresponds to the two-dimensional (2D) resistance $\rho_0^{2D} \approx 8.3k\Omega/\square$ per CuO_2, close to the universal 2D value $h/4e^2 \simeq 6.5k\Omega/\square$ [18–20]. Similar results were also found in the Zn-substituted hole-doped cuprates [21]. Moreover, the 2%–4% of Zn substitution needed to suppress completely superconductivity in $\mathrm{La_{2-x}Sr_xCu_{1-z}Zn_zO_4}$ [21] is similar to the value of 1.2%–2.3% Cu vacancies estimated in the AG and non-SC $\mathrm{Pr_{0.88}LaCe_{0.12}CuO_4}$ samples [11].

We caution that there are other possible explanations to account for the antinodal LEG, such as a charge density wave induced by the nesting of two sides of the M-centered electron pockets. However, it would then be hard to explain why both the long-range AF and this charge density wave are suppressed in the reduced samples. The unexpected presence of the antinodal LEG calls for further theoretical and experimental studies.

We are indebted to A.-M. S. Tremblay and D. Sénéchal for useful discussions. We acknowledge support from NSF Grant No. DMR-0353108, DOE Grant No. DEFG02-99ER45747 and No. DE-FG02-05ER46202. This work is based upon research conducted at the Synchrotron Radiation Center supported by NSF No. DMR-0537588. P. F. acknowledges the support of NSERC (Canada), FQRNT (Québec), CFI and CIAR.

*richarpi@bc.edu

[1] E. Moran *et al.*, Physica (Amsterdam) **160C**, 30 (1989).
[2] J. S. Kim and D. R. Gaskell, Physica (Amsterdam) **209C**, 381 (1993).
[3] E. Wang *et al.*, Phys. Rev. B **41**, 6582 (1990).
[4] E. Takayama-Muromachi *et al.*, Physica (Amsterdam) **159C**, 634 (1989).
[5] K. Susuki *et al.*, Physica (Amsterdam) **166C**, 357 (1990).
[6] J. Gauthier *et al.*, Phys. Rev. B **75**, 024424 (2007).
[7] Pengcheng Dai *et al.*, Phys. Rev. B **71**, 100502 (2005).
[8] P. Richard *et al.*, Phys. Rev. B **72**, 184514 (2005).
[9] G. Riou *et al.*, Phys. Rev. B **69**, 024511 (2004).
[10] P. Richard *et al.*, Phys. Rev. B **70**, 064513 (2004).
[11] H. J. Kang *et al.*, Nat. Mater. **6**, 224 (2007).
[12] H. Matsui *et al.*, Phys. Rev. Lett. **94**, 047005 (2005).
[13] D. K. Sunko and S. Barišić, Phys. Rev. B **75**, 060506 (2007).
[14] K. Kurahashi *et al.*, J. Phys. Soc. Jpn. **71**, 910 (2002).
[15] M. Matsuura *et al.*, Phys. Rev. B **68**, 144503 (2003).
[16] Z. Wang and P. A. Lee, Phys. Rev. Lett. **89**, 217002 (2002).
[17] S. Ouazi *et al.*, Phys. Rev. Lett. **96**, 127005 (2006).
[18] T. Pang, Phys. Rev. Lett. **62**, 2176 (1989).
[19] M. P. A. Fisher *et al.*, Phys. Rev. Lett. **64**, 587 (1990).
[20] V. J. Emery and S. A. Kivelson, Phys. Rev. Lett. **74**, 3253 (1995).
[21] Y. Fukuzumi *et al.*, Phys. Rev. Lett. **76**, 684 (1996).